

Effects of Step and Cavity Shapes on Aeration and Energy Dissipation Performances of Stepped Chutes

Gangfu Zhang¹ and Hubert Chanson²

Abstract: The effects of step edge and cavity shapes on skimming flow properties were investigated in a large-size 45° stepped chute model configured with uniform triangular steps, partially blocked cavities, and chamfers. The focus of this experimental study was the air–water flow regime and the energy dissipation performances. Visually, the partial cavity blockage and chamfers were respectively associated with an increase and a decrease in flow stability, while causing no substantial change in the general flow regimes. Comparisons of characteristic air–water properties indicated better aeration performance for the sharp edges than for the chamfers. A substantial reduction in friction factor was observed with the chamfers, while partial cavity blockages appeared to slightly improve flow resistance. A strongly negative correlation between total air entrainment and flow resistance was identified, which was more observable for the sharp edges. A comparative study revealed that sparsely spaced sharp edges at slopes between 30 and 45° might be optimal in terms of aeration and energy dissipation performances. DOI: [10.1061/\(ASCE\)HY.1943-7900.0001505](https://doi.org/10.1061/(ASCE)HY.1943-7900.0001505). © 2018 American Society of Civil Engineers.

Author keywords: Free-surface aeration; Flow resistance; Stepped spillway; Cavity geometry; Chamfer; Physical modeling; Skimming flow; Drag reduction.

Introduction

Stepped spillways have been used for several centuries to facilitate the safe passage of flood waves in dams (Chanson 2001a). The steps induce strong turbulence dissipation responsible for a significant reduction of kinetic energy in the flow above the spillway, which in turn helps protect the downstream stilling structures. In recent years, the interest in step spillway design and research grew as a result of advancement in construction techniques, including the use of roller compacted concrete (Chanson 2001a). A properly designed spillway may enable a significant reduction in stilling basin length to achieve substantial cost savings.

The aeration and energy dissipation performances of stepped chutes with flat triangular steps were extensively studied and understood, with several design guidelines proposed (e.g., Matos 2000; Chanson 2001a; Ohtsu et al. 2004; Gonzalez and Chanson 2007). On the other hand, tests performed on nonstandard configurations, such as gabions, pooled steps, and nonuniform steps, have reported changes in flow patterns, air entrainment, and energy dissipation from a standard design (e.g., Stephenson 1988; Gonzalez and Chanson 2008; Felder and Chanson 2014; Wuthrich and Chanson 2014; Zhang and Chanson 2016a). While these investigations highlighted the importance of bottom geometry in determining the characteristics of stepped chute flows, their conclusions had not always been consistent. For example, Takahashi et al. (2008) found a larger energy loss for steps with end sills at 30° relative to horizontal steps, whereas Felder and Chanson (2013) observed otherwise for 26.6° chutes. The discrepancy suggests that the performance of

stepped chutes likely results from complex interactions between the roughness geometry and flow conditions, rather than from the steps alone.

To better understand these effects, an analogy may be drawn between stepped chute flows and those past roughness strips which are commonly classified into a d- or a k-type (Gonzalez and Chanson 2004). The generally accepted classification depends on the characteristic roughness density expressed in terms of the roughness size and hydraulic diameter (e.g., Chow 1959). A decrease in roughness density may cause a shift in the mean velocity profile as well as promote vortex shedding into the overflow, as the mutual blockage between adjacent roughness elements is reduced (Perry et al. 1969). Recent numerical results (Leonardi et al. 2007) have demonstrated further possibilities to alter the relative contributions of skin friction and form drag to the total flow resistance, thus modulating the spillway performance. Such effects could also be achieved by modifying the step shape, for example, by adding chamfers, which drastically increases the crest length over which skin friction may occur and provides an additional separation point compared to a sharp edge.

The present study was motivated by these observations and aims to investigate the effects of step shape and cavity geometry in a 45° steep chute. The model configuration is typical of a gravity dam, and the slope was chosen to maintain symmetry in the cavities. Geometric variations were introduced by providing partial blockages to the step cavities and adding chamfers to the baseline case with flat triangular steps. Detailed visual observations were performed and the comparative aeration and energy dissipation performances were examined. The results revealed slight to moderate changes in flow patterns, aeration, and energy dissipation due to changes in step and cavity shapes.

Experimental Setup

The experiments were conducted in a large-size stepped spillway model (1 m wide) downstream of a 1.2 × 0.6-m (height × length) broad-crested weir. The discharge was supplied by three

¹Postdoctoral Research Fellow, School of Civil Engineering, Univ. of Queensland, Brisbane QLD 4072, Australia (corresponding author). Email: g.zhang3@uq.edu.au

²Professor, School of Civil Engineering, Univ. of Queensland, Brisbane QLD 4072, Australia. Email: h.chanson@uq.edu.au

Note. This manuscript was submitted on June 30, 2017; approved on March 26, 2018; published online on June 28, 2018. Discussion period open until November 28, 2018; separate discussions must be submitted for individual papers. This paper is part of the *Journal of Hydraulic Engineering*, © ASCE, ISSN 0733-9429.

Table 1. Experimental channel details

Model	h (m)	l (m)	λ (m)	k (m)	λ/k	θ (degrees)	Modification
I	0.1	0.1	0.14	0.071	2	45	Smooth triangular cavities (i.e., no modification)
IIa	0.1	0.1	0.14	0.047	3	45	Partially filled cavities
IIb				0.035	4		
IIc				0.024	6		
III	0.1	0.1	0.14	0.061	2.33	45	Chamfered step edges

Note: h = vertical step height; l = step length; λ = roughness wavelength = $(h^2 + l^2)^{0.5}$; k = roughness height; and θ = chute slope.

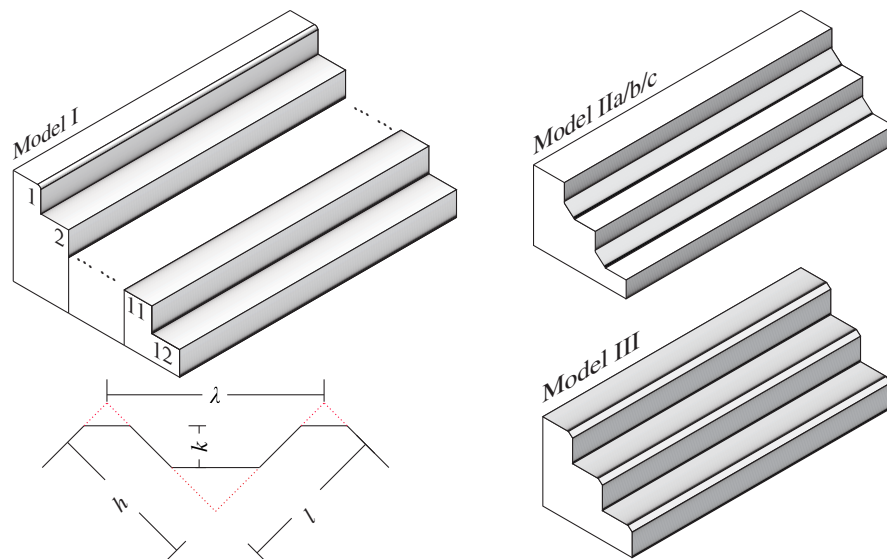
adjustable-frequency alternating current (AC) pumps. A smooth and waveless inflow was observed on the weir crest downstream of a 2.8-m-long 5.08:1 sidewall convergent. The discharge was obtained by integrating the velocity profiles measured at the centerline. Further details on the inflow conditions and broad-crested weir calibration can be found in the work of Zhang and Chanson (2016b).

Air-entrainment and energy dissipation measurements were performed in a 45° chute downstream of the broad-crested weir. The chute configurations are summarized in Table 1 and illustrated in Fig. 1. The base model consisted of 12 identical triangular steps (Fig. 1, Model I), each measuring $0.1 \times 0.1 \times 1$ m. Further investigations were undertaken by partially blocking the triangular step cavities (Fig. 1, Model IIa/b/c) and by replacing the sharp edges with 20-mm chamfers (Fig. 1, Model III). The geometric modifications were undertaken to introduce changes in the roughness density λ/k (Fig. 1), where λ is the step wavelength and k is the step roughness height, which was believed to influence mean velocity profiles, vortex shedding behaviors, and types of friction (Perry et al. 1969; Leonardi et al. 2007).

The present study mainly focused on the skimming flow regime, with model discharges between $Q = 0.083$ and 0.216 m³/s ($Re = 3.4$ – 8.8×10^5). The two-phase flow properties were recorded with dual-tip phase-detection probes (with an inner tip diameter of 0.25 mm), with longitudinal tip separations Δx between 4.3 and 8 mm. For all experiments, the sampling rate and duration were 20 kHz and 45 s respectively. A summary of the experimental flow conditions is provided in Table 2.

General Flow Observations

Visual observations identified three distinct flow regimes with largely identical flow patterns in all configurations. Detailed notes on all setups are provided in Table 3. For each setup, a nappe flow, a transition flow, and a skimming flow occur in order with increasing discharge. The nappe flow was typically characterized by a succession of jet impacts from one step edge to the next, in addition to a prominent clear water jet deflected off Step edge 2. Little to no recirculation was observed upstream of each

**Fig. 1.** Roughness configurations used in the present study.**Table 2.** Experimental flow conditions for detailed clear-water and air–water flow measurements

Model	θ (degrees)	h (m)	W (m)	λ/k	Location	Q (m ³ /s)	d_c/h	Re
I	45	0.1	1.0	2	Step edges 5–12	0.057–0.216	0.70–1.70	2.3 – 8.8×10^5
IIa	45	0.1	1.0	3	Step edges 4–12	0.083–0.216	0.90–1.70	3.4 – 8.8×10^5
IIb	45	0.1	1.0	4	Step edges 4–12	0.083–0.216	0.90–1.70	3.4 – 8.8×10^5
IIc	45	0.1	1.0	6	Step edges 4–12	0.083–0.216	0.90–1.70	3.4 – 8.8×10^5
III	45	0.1	1.0	2.33	Step edges 5–12	0.083–0.182	0.90–1.50	3.4 – 7.3×10^5

Table 3. Summary of flow regimes and transitions between flow regimes

λ/k^{*1}	h (m)	θ (degrees)	d_c/h	Regime	Comment	Note
2	0.1	45	0–0.15	NA I	Fragmented flow	Model I, triangular steps and cavities
			0.15–0.4	NA II	Clear jet at Step 2	
			0.4–0.6	TRA I	Jet + partially filled cavities	
			0.6–0.9	TRA II	Partially filled cavities	
			>0.9	SK	All cavities filled	
2.33	0.1	45	0–0.1	NA I	Fragmented flow	Model III, chamfered steps and triangular cavities
			0.1–0.5	NA II	Clear jet at Step 2	
			0.5–0.65	TRA I	Jet + partially filled cavities	
			0.65–0.9	TRA II	Partially filled cavities	
			>0.9	SK	All cavities filled	
3	0.1	45	0–0.1	NA I	As for $\lambda/k = 2$	Model IIa, triangular steps and trapezoidal cavities
			0.1–0.6	NA II	As for $\lambda/k = 2$, first two step cavities filled	
			0.6–0.9	TRA II	As for $\lambda/k = 2$	
			>0.9	SK	As for $\lambda/k = 2$	
4	0.1	45	0–0.6	NA II	Clinging nappe on Step 1	Model IIb, triangular steps and trapezoidal cavities
			0.6–0.9	TRA II	As for $\lambda/k = 2$	
			>0.9	SK	As for $\lambda/k = 2$	
6	0.1	45	0–0.6	NA II	As for $\lambda/k = 2$	Model IIc, triangular steps and trapezoidal cavities
			0.6–1.0	TRA II	As $\lambda/k = 2$	
			>1.0	SK	As $\lambda/k = 2$	

Note: $1 - \lambda =$ step wavelength; and $k =$ step roughness height.

nappe impact, contrary to observations for flat to moderate chute slopes (e.g., Toombes and Chanson 2008). The transition flow occurs for an intermediate range of discharges and exhibits some strong visual instabilities in all setups. The step cavities were either fully or partially filled, consistent with previous studies (e.g., Chanson and Toombes 2004). The deflecting jet at Step edge 2 disappeared at the upper range of transition flow discharges. For the largest discharges, the skimming flows in all setups exhibited a wavy free-surface profile approximately in phase with the stepped bottom. The cavities were occupied by stable recirculations, and irregular ejections and replacements of fluid from and into the cavity were observed in a manner similar to that found by Djenidi et al. (1999), Chanson and Toombes (2002a), and Chanson et al. (2002), highlighting the strong mainstream-cavity interactions.

Notes on Modified Setups (Model IIa/b/c and Model III)

In Model IIa/b/c, a reduction in the roughness density λ/k was achieved by partially blocking the step cavities (Fig. 1). The introduced blockage appeared to resist the fluid buildup within the step cavity, thereby prolonging the lifespan of a nappe regime [Fig. 2(a)], in which stronger splashes were observed compared to the baseline case. On the other hand, the skimming flow regime in Model IIa/b/c/ showed little difference from Model I [Fig. 2(b)]. A closer inspection revealed stronger flow projections above the mainstream, and ejections of slightly increased frequency/energy from the cavities into the mainstream. For a range of lower discharges, some transverse free-surface undulations were evident when observed from upstream [Fig. 2(c)], which was not obvious in the base model. With increasing blockage, the recirculating fluid in the cavity gradually reduced in symmetry, and displayed a corresponding increase in chaotic behaviors characterized by irregular ejections and replenishments of fluid from and into the cavity [Fig. 2(d)]. The visual instabilities were associated with the observed onset of free-surface aeration typically one step further upstream than the unmodified chute.

In Model III, the chamfers caused a slight reduction in cavity size (i.e., losing the edges) and a large increase in roughness crest length relative to the base case. The flow patterns and demarcations between

flow regimes were essentially identical to the base case with flat steps [Figs. 2(e and f), Table 3], with the exception of a slightly smoother overflow at large discharges. Both mainstream and cavity flows were visually very stable, and the onset of free-surface aeration typically occurred one to several steps further downstream than the unmodified chute. Overall, the present observations tend to suggest slight to moderate modifications to various visual aspects of stepped chute flow due to step and cavity modifications.

Free-Surface Aeration

Inception Point Location

The inception point locations in all models were determined visually and are presented in Fig. 3(a) as a function of the dimensionless discharge F^* , given as

$$F^* = \frac{q_w}{\sqrt{g \sin \theta k^3}} \quad (1)$$

where $q_w =$ discharge per unit width; $g =$ gravity constant; and $\theta = 45^\circ$ is the chute slope. The sharp edge data (I, IIa, IIb, IIc) were best correlated by

$$\frac{x_i}{k} = 2.2F^* + 3.57 \quad \text{for sharp edges, } R = 0.99 \quad (2)$$

In comparison, the chamfer data (Model III) exhibited a significant downstream shift of the inception point location. All present data were overestimated by the model of Chanson (1994), while the chamfer data displayed a reasonable agreement with Meireles et al. (2012) (for a 53° chute). Importantly, the present observations indicated substantial effects of step edge shape on the inception point location.

The corresponding clear water depth d_i is presented in Fig. 3(b). A good correlation was observed between the present data and those of Chanson (1994), given as

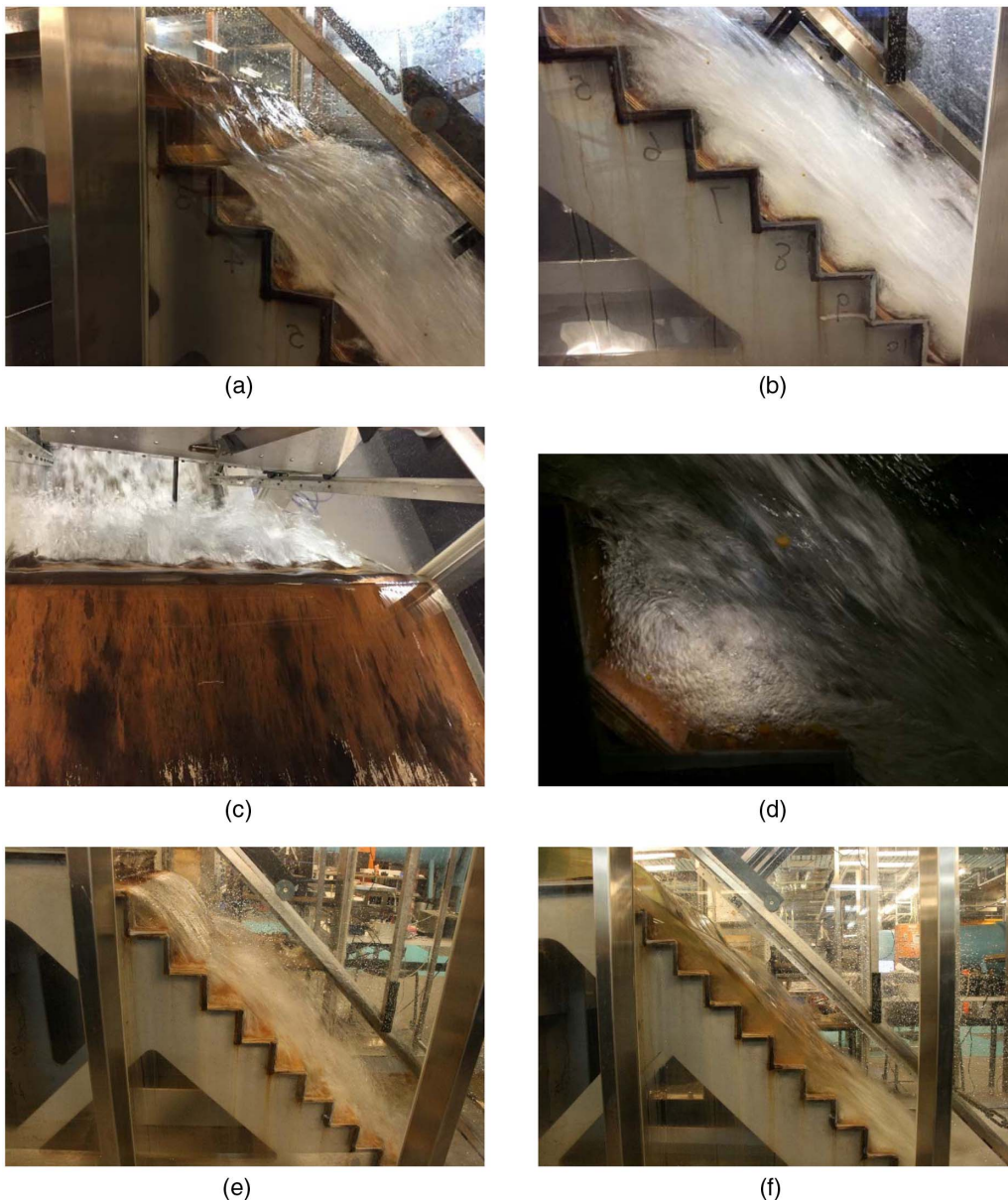


Fig. 2. Flow patterns on stepped chutes with modified steps and cavities: (a) nappe flow ($d_c/h = 0.52$, Model IIa); (b) skimming flow ($d_c/h = 1.17$, Model IIa); (c) transverse waves ($d_c/h = 0.52$, Model IIa); (d) cavity recirculation ($d_c/h = 0.77$, Model IIa); (e) nappe flow ($d_c/h = 0.18$, Model III); and (f) skimming flow ($d_c/h = 1.33$, Model III).

$$\frac{d_i}{k} = \frac{0.4034}{(\sin \theta)^{0.04}} F^{*0.592} \quad (3)$$

The result showed that the depth at inception was a function of chute slope, step roughness, and discharge; the step edge and bed-form appeared to bear no significant effect on d_i .

Downstream Air–Water Properties

The comparative performances of the models were investigated by examining the air–water flow properties at the downstream end of the chute (Step edge 12). Note that the chute length, number of steps, and drop height (10 cm) were kept constant during all comparisons, and uniform equilibrium flows were not achieved. Fig. 4(a) presents the depth-averaged mean air concentration C_{mean} in all models at Step edge 12, where

$$C_{\text{mean}} = \int_0^{Y_{90}} C dy \quad (4)$$

The results showed a decrease in C_{mean} with increasing discharge, resulting from a delayed onset of aeration. The sharp edge data exhibited consistently higher C_{mean} values in comparison to the chamfer data, which could reflect modifications to the turbulent wakes behind step edges. The partial cavity blockages (Model IIa/b/c) appeared to cause some data scatter associated with changes to the underlying states of vortex shedding. Overall, the mean air concentration data exhibited some sensitivity to the step edge profile and, to a lesser extent, the cavity shape (i.e., λ/k).

Fig. 4(b) presents the equivalent clear water depth [$d_c = (1 - C_{\text{mean}})Y_{90}$] and characteristic air–water flow depths (Y_{50} , Y_{90}) at Step edge 12. For all sharp edge models, the equivalent clear water depth d_c and air–water depth Y_{50} remained close to

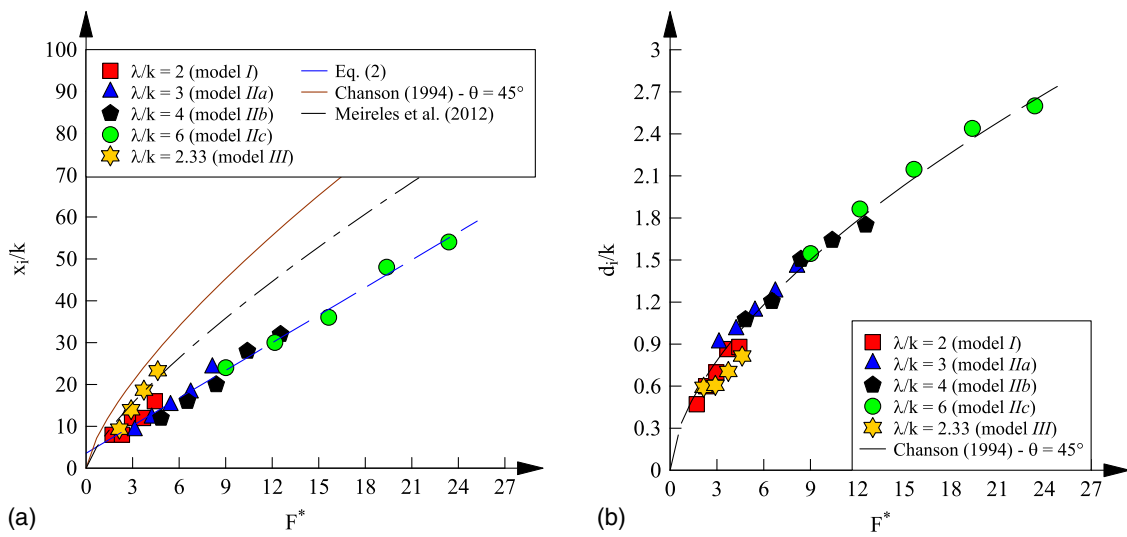


Fig. 3. Location of and flow depth at inception point of free-surface aeration—flow conditions: $\lambda/k = 2, 2.33, 3, 4, 6$; $d_c/h = 0.9, 1.1, 1.3, 1.5, 1.7$; $\theta = 45^\circ$; $h = 0.1$ m: (a) location of inception point; and (b) flow depth at inception point.

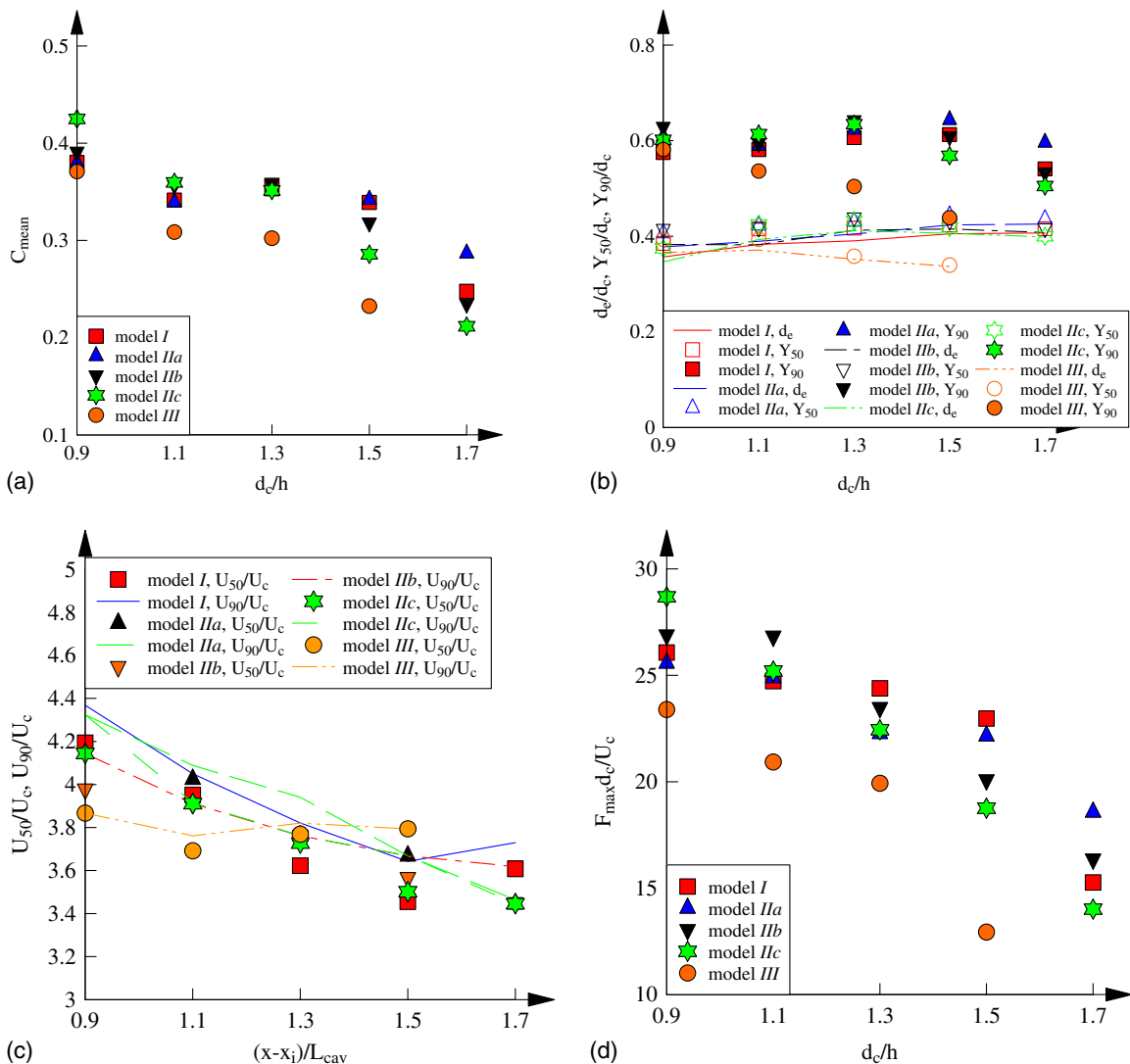


Fig. 4. Comparison of air-water flow properties at the downstream end of the chute between stepped models, with data for Model III taken at the downstream edge of chamfer: (a) depth-averaged air content (C_{mean}); (b) flow depths (d_e, Y_{50}, Y_{90}); (c) characteristic velocity (U_{50}, U_{90}); and (d) maximum bubble count rate (F_{max}).

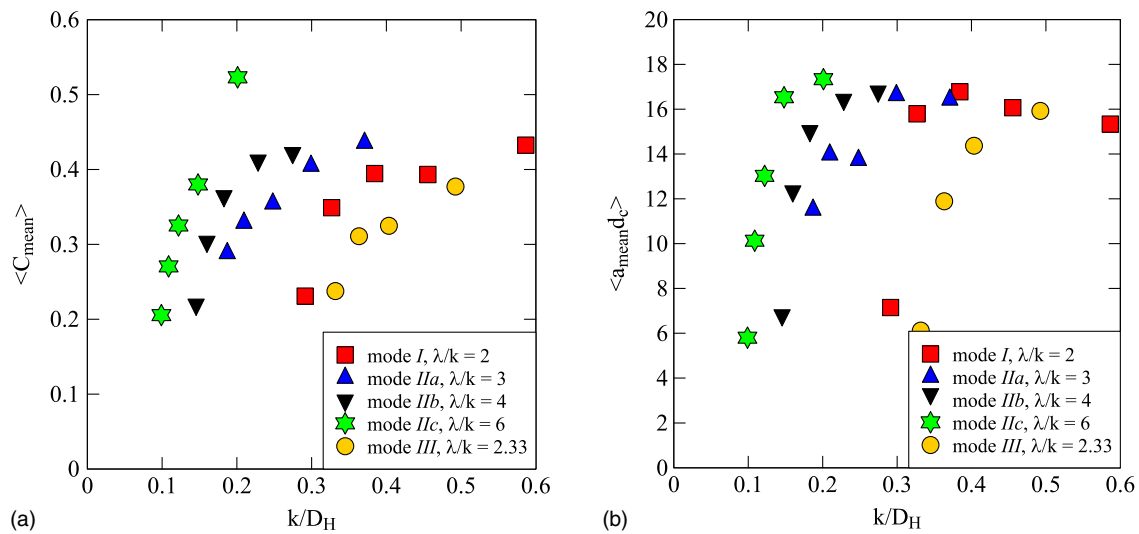


Fig. 5. Comparison of aeration performance between different stepped models—flow conditions: $d_c/h = 0.9, 1.1, 1.3, 1.5, 1.7$; $\lambda/k = 2, 3, 4, 6$; $d_c/h = 0.9, 1.1, 1.3, 1.5$; $\lambda/k = 2.33$; $\theta = 45^\circ$: (a) double-averaged mean void fraction; and (b) double-averaged specific interfacial area.

$0.4d_c$ regardless of the discharge. On the other hand, both d_e and Y_{50} decreased with increasing discharge in the chamfered setup, reflecting a reduction in energy dissipation performance at large discharges. The air–water height Y_{90} may be regarded as a typical *spray height*, which remained close to $1.5d_c$ in all sharp edge models. A closer inspection revealed consistently larger spray height in Model IIa than in Model I, which could be linked to more energetic cavity ejections due to a reduction in mutual sheltering, though this was not obvious in Models IIb and IIc, possibly as a consequence of their smaller roughness sizes.

Fig. 4(c) compares the downstream characteristic mixture velocities U_{50} and U_{90} between all models. All but the chamfer data (Model III) displayed decreasing air–water velocities with increasing discharge, with little observable difference limited to cavity modifications. For the chamfer model, the U_{50} and U_{90} data were insensitive to discharge—both remaining at approximately $3.8U_c$. The finding suggested that the kinetic energy head in a chamfered chute might scale poorly with discharge.

Fig. 4(d) compares the cross-sectional maximum bubble count rate at the downstream end of the chute. All data showed a significant reduction in bubble count rate with increasing discharge because of delayed free-surface aeration. Similar levels of F_{max} were recorded between the sharp edge models, which consistently exceeded the chamfered chute values. The observation could be a result of less air entrainment (i.e., C_{mean}) coupled with lower turbulent stress levels in the chamfered chute.

The present comparisons suggest that (1) the sharp edge data were consistent with previous studies (e.g., Chanson 1993; Chamani and Rajaratnam 1999; Chanson 2001b; Matos 2000; Ohtsu et al. 2004; Felder 2013) and (2) there were higher air entrainment and energy dissipation performances for sharp edges than for chamfers.

Total Aeration

Aeration performances of stepped chutes are drastically improved over conventional smooth chutes because of enhanced turbulent mixing, increased air–water interfacial area, and larger flow resistance that improves the residence time of the flow (Toombes 2002). The total amount of air entrainment in the aerated flow region may be estimated by double-averaging the mean air concentration:

$$\langle C_{\text{mean}} \rangle = \frac{1}{Y_{90}(x_e - x_i)} \int_{x_i}^{x_e} \int_0^{Y_{90}} C dy dx \quad (5)$$

where x_i and x_e = streamwise coordinates of the inception point and the last step edge respectively. Fig. 5(a) presents $\langle C_{\text{mean}} \rangle$ in all stepped chutes as a function of the relative roughness k/D_H (D_H is obtained at the last step edge). In all models, the total amount of air entrainment increased rapidly with relative roughness because of enhanced turbulent transport. The required relative roughness k/D_H for reaching a target level of $\langle C_{\text{mean}} \rangle$ increased with decreasing λ/k , and it was the largest for the chamfered steps. This suggests that sharp edges with large λ/k are most conducive to air entrainment. Note that the large k/D_H values implied a strong dependence of air entrainment on the individual roughness characteristics.

A further parameter for assessing the aeration performance of stepped chutes is the specific interfacial area a_i proportional to the rate of air–water mass transfer. Herein, a_i was estimated from the phase-detection probe data according to Toombes (2002) as follows:

$$a_i = 4F/U_{\text{aw}} \quad (6)$$

In Eq. (6), a_i scales directly with the bubble count rate F and the flow residence time proportional to $1/U_{\text{aw}}$. Thus, a large number of smaller bubbles coupled with a long residence time improve the air–mass transfer on a stepped chute. Fig. 5(b) presents the double-averaged specific interfacial area $\langle a_i \rangle$ in all setups, calculated as

$$\langle a_{\text{mean}} \rangle = \frac{1}{Y_{90}(x_e - x_i)} \int_{x_i}^{x_e} \int_0^{Y_{90}} a_i dy dx \quad (7)$$

which is proportional to the rate of air–water mass transfer in the entire aerated region. For all chutes, the dimensionless double-averaged specific interfacial area $\langle a_{\text{mean}} d_c \rangle$ displayed an initial rapid increase with k/D_H before reaching a plateau at about $\langle a_{\text{mean}} d_c \rangle = 16$. Typically, a smaller roughness k/D_H is required to achieve a target interfacial area in a sharp edge model than in the chamfered model. For a given interfacial area, k/D_H increased with decreasing λ/k for the sharp edge models. The observations implied that sharp edge models with large λ/k are the most efficient in terms of air–water mass transfer.

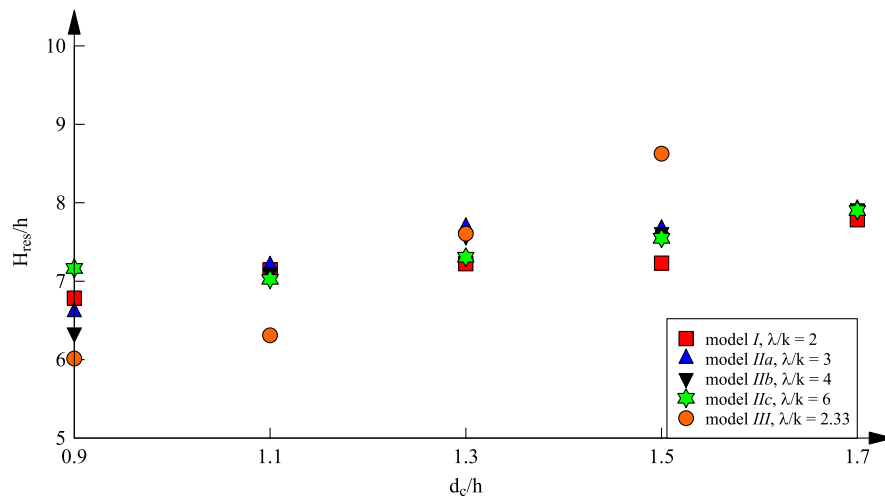


Fig. 6. Residual head for all stepped spillway models—flow conditions: $d_c/h = 0.9, 1.1, 1.3, 1.5, 1.7$; $\lambda/k = 2, 3, 4, 6$; $d_c/h = 0.9, 1.1, 1.3, 1.5$; $\lambda/k = 2.33$; $\theta = 45^\circ$. Comparison with median values from Felder and Chanson (2009).

Energy Dissipation

Residual Head

The residual head (H_{res}) data recorded at the downstream end of the chute (Step edge 12) are compared between all models in Fig. 6. The data were obtained from depth-averaging the phase detection probe data as follows:

$$H_{res} = \frac{1}{d_c} \int_0^{Y_{90}} H_t dy \quad (8)$$

where

$$H_t = (1 - C) \left(\frac{U_{aw}^2}{2g} + z \right) + H_s \quad (9)$$

where U_{aw} = mixture velocity; and H_s = pressure head obtained by assuming a hydrostatic pressure distribution between $y = 0$ and $y = Y_{90}$. Note that, for a given discharge, the minimum residual head is governed by the critical flow condition

$$\frac{H_{res,min}}{h} = 1 + 1.5 \frac{d_c}{h} \quad (10)$$

For all data, the residual head H_{res} exhibited an approximately linear increase with increasing discharge, with a slightly higher rate of increase observed for the chamfer data. The sharp edge data were relatively consistent, indicating that the cavity shape had only minor influences on the residual head. Qualitatively, the largest residual head ($H_{res}/h = 8.7$, $d_c/h = 1.5$) was recorded with the chamfers, which might reflect a moderate drag reduction at higher discharges. All present data were larger than the median values for slopes up to 26.6° provided in Felder and Chanson (2009), though differences in chute lengths were not accounted for. The comparison indicated some slope effect on the energy dissipation performance.

Friction Factor

The high rate of energy dissipation on stepped chutes encompassed a dominant form loss contribution. Depending upon the bottom geometry, large skin friction might occur at several locations, including immediately downstream of the overflow impingement

on the step face and above the chamfer crest. The total flow resistance in quasismooth skimming flows is typically characterized using the Darcy-Weisbach friction factor (Rajaratnam 1990; Chanson 2001b)

$$f = \frac{8S_f d_c^3}{d_c^3} \quad (11)$$

where $S_f = -dH_t/dx$ is the friction slope; d_e = equivalent clear water depth deduced from the void fraction profile (i.e., $d_e = \int_0^{Y_{90}} (1 - C) dy$); and d_c = critical depth. The present data are summarized in Fig. 7, in which they are grouped according to the flow regions indicated by different subscripts (cw = clear water, e = air-water, all = whole chute). Note that f_{cw} , f_e , and f_{all} respectively represent the average values for the clear water region, aerated region, and the whole chute. For completeness, the step-induced form drag was derived from a simple mixing length model (Chanson et al. 2002) as follows:

$$f_d = \frac{2}{\sqrt{\pi K}} \quad (12)$$

where K^{-1} is proportional to the dimensionless expansion rate of the shear layer trailing each step edge. Brattberg et al. (1998) found a best fit of $K \approx 6$ for plunging jets ranging between 2 and 6 m/s, which corresponded to $f_d = 0.188$. This estimate is represented by thick black dashed lines in Fig. 7. A summary of the average friction factors in each flow region is provided in Table 4.

Fig. 7(a) presents the clear water friction factors (f_{cw}) in all models, with typical values between 0.1 and 0.3 and averaging slightly below the mixing length model estimate (0.153 versus 0.188). Slightly larger f_{cw} were observed in the models with partial cavity blockages that might have reflected some enhanced mainstream-cavity interactions. For the reference model (I), f_{cw} was a decreasing function of k/D_H , which might imply some Reynolds number dependence. Overall, the present data were consistent with previous observations (Amador 2005; Meireles 2011; Frizell et al. 2013).

Downstream of the inception point, the air-water friction factors (f_e) calculated for all models ranged between 0.1 and 0.4 [Fig. 7(b)], which showed increases from their respective clear water values. The average air-water friction factors for the sharp edge and chamfer models were 0.28 and 0.22 respectively (Table 4), highlighting the sensitivity of flow resistance to the step shape.

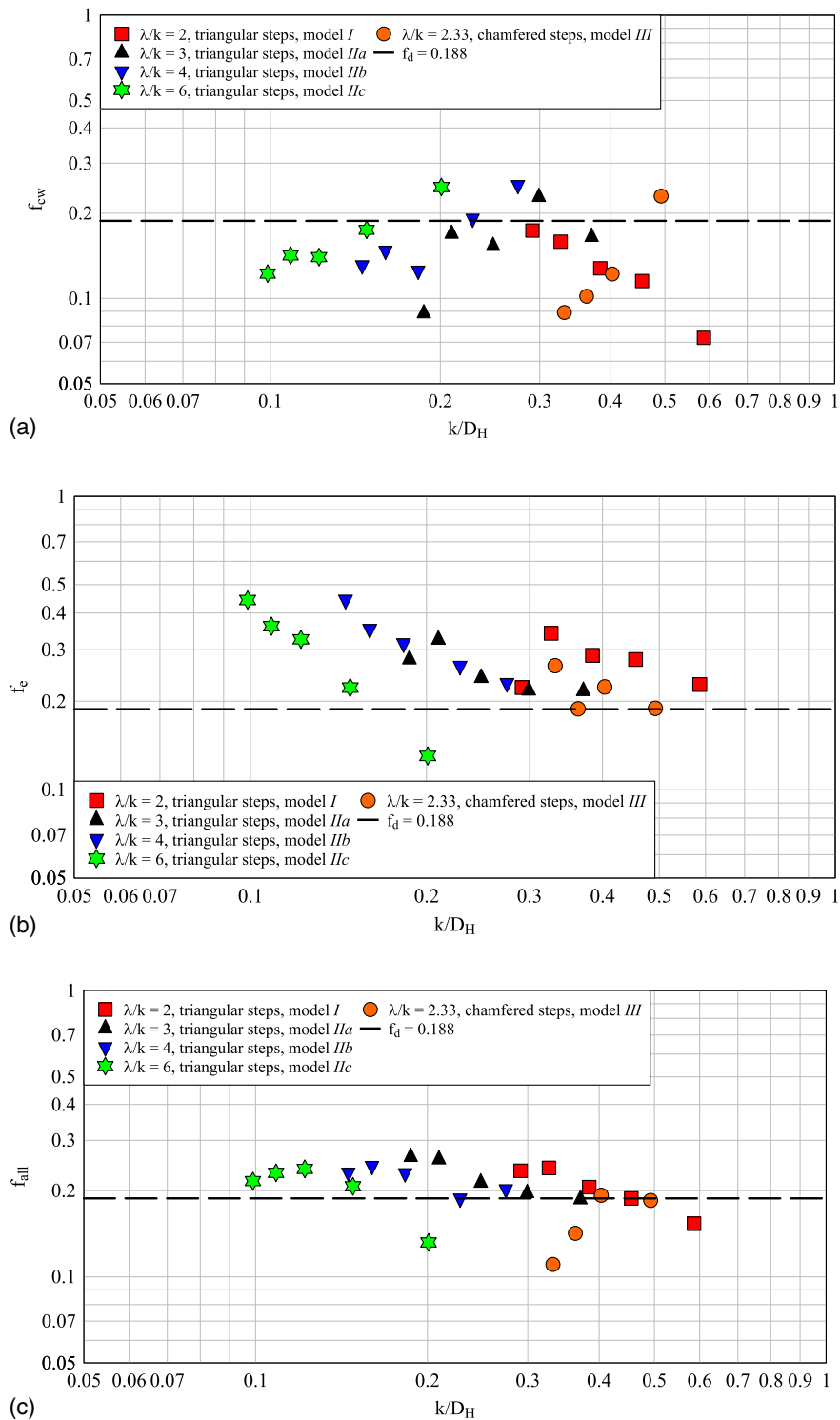


Fig. 7. Friction factors in the developing clear water flow region, fully developed aerated flow region, and whole chute in all stepped models—flow conditions: $d_c/h = 0.9, 1.1, 1.3, 1.5, 1.7$; $\lambda/k = 2, 3, 4, 6$; $d_c/h = 0.9, 1.1, 1.3, 1.5$; $\lambda/k = 2, 3.3$; $\theta = 45^\circ$: (a) developing clear water flow region; (b) fully developed aerated flow region; and (c) whole chute.

The decreasing trend of f_e with increasing k/D_H indicated some bubble-induced drag reduction. This drag-reducing phenomenon in skimming flows was highlighted in previous studies, including those of Matos (1999), Boes and Hager (2003), and Chanson (2004). The present data are plotted as a function of the double-averaged mean void fraction $\langle C_{mean} \rangle$ in Fig. 8, yielding the following best correlations:

$$f_e = -0.92 \langle C_{mean} \rangle + 0.62 \text{ sharp edges}, \quad R = 0.92 \quad (13)$$

$$f_e = -0.52 \langle C_{mean} \rangle + 0.38 \text{ chamfers}, \quad R = 0.84 \quad (14)$$

Despite the simplistic fits, the high correlation coefficients indicated that the reduction in f_e with increasing k/D_H was mostly

Table 4. Average friction factors in all stepped models

Model	f_{cw} (clear water)	f_e (air-water)	f_{all} (whole chute)	Remarks
I	0.130	0.271	0.204	Triangular steps, $\lambda/k = 2$
IIa	0.161	0.256	0.223	Partial cavity blockage, $\lambda/k = 3$
IIb	0.169	0.321	0.219	Partial cavity blockage, $\lambda/k = 4$
IIc	0.165	0.296	0.205	Partial cavity blockage, $\lambda/k = 6$
III	0.136	0.217	0.157	20-mm chamfers

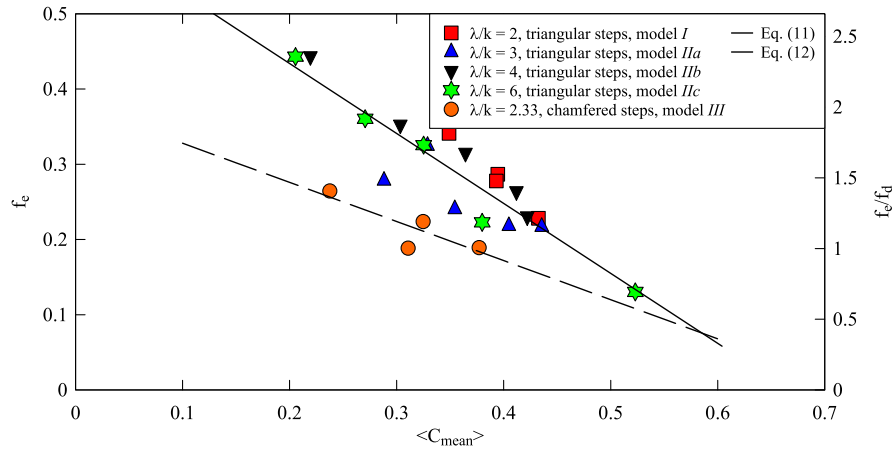


Fig. 8. Drag reduction in skimming flows.

explained by air entrainment. At a given $\langle C_{mean} \rangle$, the chamfer data yield a lower f_e than the sharp edges. Lastly, $\langle C_{mean} \rangle$ had a much larger influence on f_e for sharp edges than for chamfers, indicating some sensitivity to the step edge profile. Overall, the flow resistance was the largest for the sharp edge models despite some evidence of drag reduction.

Fig. 7(c) presents the average friction factors over the entire chute length (f_{all}) for all models. All data ranged between 0.1 and 0.3 and were comparable to the analytical estimate f_d . The models with partially blocked cavities and with chamfers were respectively associated with the highest and lowest average values of f_{all} (Table 4). The finding showed that sharp edges and partial cavity blockage might improve the energy dissipation performance of stepped chutes.

Discussion

Flow resistance in skimming flows consists of form drag generated by the step edges and skin friction occurring on the downstream end of each step. For stepped chutes with uniform triangular steps, the ratio between form drag and skin friction contributions is a function of the chute slope θ . The present data are compared to the air-water friction factors obtained for chute slopes $3.4 \leq \theta \leq 59^\circ$ in Fig. 9. Details of experimental data are provided in the Appendix. Despite some scatter, the data exhibited a general trend of decreasing friction with decreasing chute slope. The average of all data ($f_{e,avg} = 0.190$) was comparable to that estimated by Chanson et al. (2002), adopting a simple mixing length model ($f_d = 0.188$, black dash). The friction factor data were averaged for each slope ($f_{e,mean}$) and plotted as a function of θ in Fig. 10,

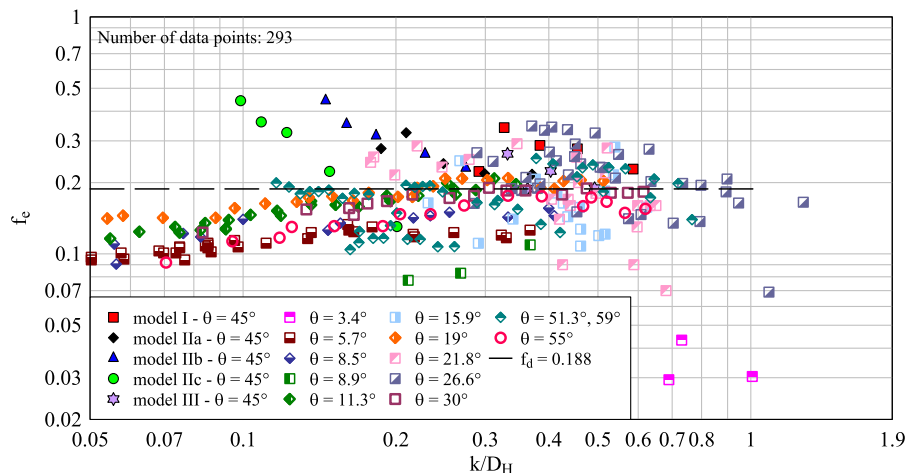


Fig. 9. Comparison of air-water friction factors between stepped chutes with different slopes.

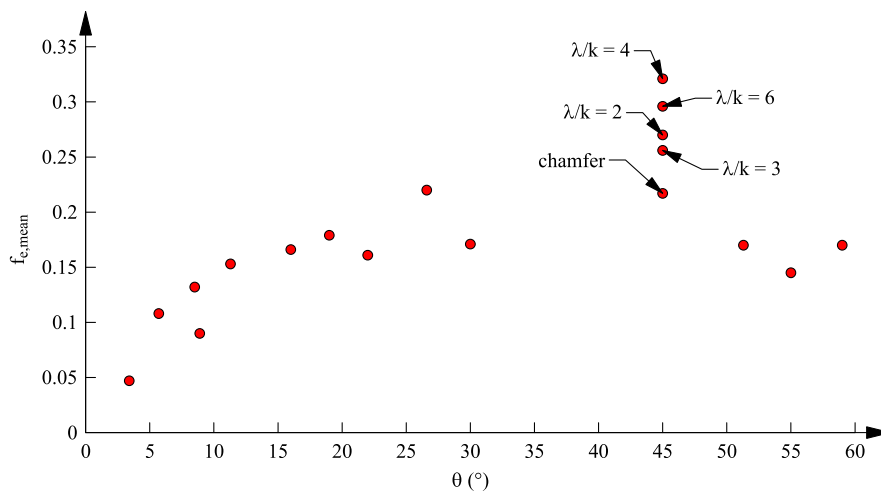


Fig. 10. Effect of chute slope on the air–water friction factor f_e .

including a total number of 293 data points. Note that the averaging approach was adopted to shed light on the typical performance of each setup under a range of flow conditions, without making attempts to account for effects due to inflow conditions, methodology, and scale. The process suggested an increasing f_e with increasing slope up to about 45° , followed by a slight decrease up to 60° . The initial trend ($3.4 \leq \theta \leq 21.8^\circ$) was consistent with the findings of Gonzalez and Chanson (2006). The optimal slope for energy dissipation might appear to be about $\theta = 20 - 45^\circ$. The present data ($\theta = 45^\circ$) also indicated generally larger f_e for small roughness densities λ/k , and smaller f_e for chamfered edges. Overall, the air–water flow resistance in stepped chutes is heavily influenced by the bottom geometry and appears to be a complex function of the state of vortex shedding.

Conclusion

Extensive physical measurements were conducted in five stepped chute models to determine their comparative performances. The work focused on the effects of step edge and step cavity configurations. The step edge and cavity geometries were found to exhibit some influences on the amount of air entrainment and flow resistance.

In all stepped models, visual observations indicated that partial cavity blockages were associated with increased overflow instabilities. This could reflect a reduction in the mutual sheltering between

adjacent steps, which resulted in a slightly earlier onset of free-surface aeration compared to unmodified triangular steps for a given discharge. Conversely, chamfering the steps caused a downstream shift in the inception point location as well as a visually smooth overflow. Examinations of the double-averaged mean void fraction and double-averaged specific interfacial area suggested that the sharp edge models with partially blocked cavities were superior in terms of both air-entrainment and air–water mass transfer.

The residual head data suggested similar levels of energy dissipation between the sharp edge models. Comparatively, the residual head on the chamfer model was most sensitive to discharge and was the largest among all setups for $d_c/h \geq 1.3$. For each setup, the flow resistances in the developing flow region, aerated flow region, and the whole chute were analyzed individually. Partial cavity blockages and chamfers were found to increase and reduce the flow resistance respectively. A significant drag reduction was observed in the aerated flow region and was strongly correlated with the total amount of air entrained ($\langle C_{mean} \rangle$). Further comparisons with previous studies revealed significant slope effects on energy dissipation, with $\theta = 20 - 45^\circ$ found to be the optimal range. Overall, the present data suggest that, for a fixed drop height h , the energy dissipation performance improves for sharp edges and increased sparsity λ/k , although the nonstandard design may lead to a complicated and expensive construction process.

Appendix. Summary of Air–Water Friction Data on Stepped Chutes

Flow resistance in skimming flows over stepped chutes is governed by the chute slope θ , as well as influenced by the step and cavity geometries. The present data are compared to previous studies with slopes ranging between $\theta = 3.4^\circ$ and $\theta = 59^\circ$. The data were averaged for each slope and summarized herein.

Reference	θ (degrees)	λ/k	h (m)	W (m)	$f_{e,mean}$	Remarks
Present study	45	2	0.10	1.0	0.27	Triangular steps, uncontrolled broad crest
		3			0.26	Partial cavity blockage, uncontrolled
		4			0.32	broad crest
		6			0.30	
		2.3			0.22	20-mm chamfers, uncontrolled broad crest
Chanson and Toombes (2002b)	3.4	16.9	0.07, 0.14	0.5	0.03	Horizontal timber steps. With or without sidewall offset for nappe ventilation at first drop. Pressurized nozzle

Appendix (Continued.)

Reference	θ (degrees)	λ/k	h (m)	W (m)	$f_{e,\text{mean}}$	Remarks
Ohtsu et al. (2004)	5.7	10.1	0.00625–0.05	0.4	0.11	Uncontrolled ogee crest
Ohtsu et al. (2004)	8.5	6.8	0.00625–0.05	0.4	0.13	Uncontrolled ogee crest
Felder (2013)	8.9	6.5	0.05	0.5	0.09	Uncontrolled broad crest
Ohtsu et al. (2004)	11.3	5.2	0.00625–0.05	0.4	0.15	Uncontrolled ogee crest
Gonzalez (2005)	15.9	3.9	0.05, 0.10	1.0	0.17	Uncontrolled broad crest
Ohtsu et al. (2004)	19	3.2	0.00625–0.05	0.4	0.18	Uncontrolled broad crest
Carosi and Chanson (2006), Chanson and Toombes (2002c) and Felder and Chanson (2009)	21.8	2.9	0.05, 0.10	1.0	0.19	Uncontrolled broad crest
Felder (2013) and Wuthrich and Chanson (2014)	26.6	2.5	0.05, 0.1	0.52, 1.0	0.22	Uncontrolled broad crest
Ohtsu et al. (2004)	30	2.3	0.00625–0.05	0.4	0.17	Uncontrolled broad crest
Chamani and Rajaratnam (1999)	51.3, 59	2.0–2.3	0.125–0.313	0.3	0.17	Uncontrolled ogee crest
Ohtsu et al. (2004)	55	2.1	0.00625–0.1	0.4	0.15	Uncontrolled ogee crest

Acknowledgments

The authors acknowledge the technical assistance of Jason Van Der Gevel and Stewart Matthews (School of Civil Engineering, University of Queensland). The financial support of the Australian Research Council (Grant No. DP120100481) is acknowledged.

Notation

The following symbols are used in this paper:

- a_i = specific interfacial area (1/m);
- a_{mean} = depth-averaged specific interface area (1/m);
- C = time-averaged void fraction;
- C_{mean} = depth-averaged void fraction;
- D_H = hydraulic diameter (m);
- d_c = critical depth (m);
- d_e = equivalent clear water depth (m);
- d_i = water depth at inception point of free-surface aeration (m);
- F = bubble count rate (Hz);
- F^* = roughness Froude number;
- f_{all} = friction factor averaged over whole chute;
- f_{cw} = clear water friction factor;
- f_d = friction factor deduced from a simplified mixing length model;
- f_e = air–water friction factor;
- $f_{e,\text{mean}}$ = average air–water friction factor;
- g = gravity constant (m/s^2);
- H_{res} = residual head (m);
- H_s = pressure head (m);
- H_t = total head (m);
- h = vertical step height (m);
- K = dimensionless constant inversely proportional to shear layer expansion rate;
- k = step roughness height (m);
- L_{cav} = step cavity length (m);
- l = horizontal step length (m);
- Q = water discharge (m^3/s);
- q_w = unit discharge of water (m^2/s);
- R = normalized correlation coefficient;
- R = Reynolds number;

S_f = friction slope;

t = time (s);

U_{aw} = time-averaged interfacial velocity (m/s);

U_{50} = time-averaged interfacial velocity corresponding to $C = 0.5$ (m/s);

W = chute width (m);

x = streamwise coordinate (m);

x_e = streamwise coordinate corresponding to the end of chute (m);

x_i = streamwise position of the inception point of free-surface aeration (m);

Y_{50} = elevation normal to the pseudobottom where $C = 0.5$ (m);

Y_{90} = elevation normal to the pseudobottom where $C = 0.9$ (m);

y = normal coordinate (m);

z = elevation head (m);

Δx = streamwise separation between probe tips (m);

θ = chute slope (degrees); and

λ = streamwise separation between adjacent steps (m).

References

- Amador, A. 2005. “Comportamiento hidráulico de los aliviaderos escalonados en presas de hormigón compactado.” [In Spanish.] Ph.D. thesis, Dep. de Ingeniería Hidráulica, Marítima y Ambiental, Technical Univ. of Catalonia (UPC).
- Boes, R. M., and W. H. Hager. 2003. “Hydraulic design of stepped spillways.” *J. Hydraul. Eng.* 129 (9): 661–670. [https://doi.org/10.1061/\(ASCE\)0733-9429\(2003\)129:9\(661\)](https://doi.org/10.1061/(ASCE)0733-9429(2003)129:9(661)).
- Brattberg, T., H. Chanson, and L. Toombes. 1998. “Experimental investigations of free-surface aeration in the developing flow of two-dimensional water jets.” *J. Fluids Eng.* 120 (4): 738–744. <https://doi.org/10.1115/1.2820731>.
- Carosi, G., and H. Chanson. 2006. *Air-water time and length scales in skimming flow on a stepped spillway. Application to the spray characterisation*. Rep. No. CH59/06. Brisbane, Australia: Division of Civil Engineering.
- Chamani, M. R., and N. Rajaratnam. 1999. “Characteristics of skimming flow over stepped spillways.” *J. Hydraul. Eng.* 125 (4): 361–368. [https://doi.org/10.1061/\(ASCE\)0733-9429\(1999\)125:4\(361\)](https://doi.org/10.1061/(ASCE)0733-9429(1999)125:4(361)).
- Chanson, H. 1993. “Stepped spillway flows and air entrainment.” *Can. J. Civ. Eng.* 20 (3): 422–435. <https://doi.org/10.1139/93-057>.

- Chanson, H. 1994. "Hydraulics of skimming flows over stepped channels and spillways." *J. Hydraul. Res.* 32 (3): 445–460. <https://doi.org/10.1080/00221689409498745>.
- Chanson, H. 2001a. *The hydraulics of stepped chutes and spillways*, 418. Lisse, Netherlands: Balkema.
- Chanson, H. 2001b. "Hydraulic design of stepped spillways and downstream energy dissipators." *Dam Eng.* 11 (4): 205–242.
- Chanson, H. 2004. "Drag reduction in skimming flow on stepped spillways by aeration." *J. Hydraul. Res.* 42 (3): 316–322. <https://doi.org/10.1080/00221686.2004.9728397>.
- Chanson, H., and L. Toombes. 2002a. "Air-water flows down stepped chutes: Turbulence and flow structure observations." *Int. J. Multiphase Flow* 28 (11): 1737–1761. [https://doi.org/10.1016/s0301-9322\(02\)00089-7](https://doi.org/10.1016/s0301-9322(02)00089-7).
- Chanson, H., and L. Toombes. 2002b. "Energy dissipation and air entrainment in stepped storm waterway. Experimental study." *J. Irrig. Drain. Eng.* 128 (5): 305–315. [https://doi.org/10.1061/\(asce\)0733-9437\(2002\)128:5\(305\)](https://doi.org/10.1061/(asce)0733-9437(2002)128:5(305)).
- Chanson, H., and L. Toombes. 2002c. "Experimental investigations of air entrainment in transition and skimming flows down a stepped chute." *Can. J. Civ. Eng.* 29 (1): 145–156. <https://doi.org/10.1139/01-084>.
- Chanson, H., and L. Toombes. 2004. "Hydraulics of stepped chutes: The transition flow." *J. Hydraul. Res.* 42 (1): 43–54. <https://doi.org/10.1080/00221686.2004.9641182>.
- Chanson, H., Y. Yasuda, and I. Ohtsu. 2002. "Flow resistance in skimming flows and its modelling." *Can. J. Civ. Eng.* 29 (6): 809–819. <https://doi.org/10.1139/02-083>.
- Chow, V. T. 1959. *Open channel hydraulics*, 680. New York: McGraw-Hill.
- Djenidi, L., F. Anselmet, and R. A. Antonia. 1999. "The turbulent boundary layer over transverse square cavities." *J. Fluid Mech.* 395: 271–294. <https://doi.org/10.1017/S0022112099005911>.
- Felder, S. 2013. "Air-water flow properties on stepped spillways for embankment dams: Aeration, energy dissipation and turbulence on uniform, non-uniform and pooled stepped chutes." Ph.D. thesis, School of Civil Engineering, Univ. of Queensland.
- Felder, S., and H. Chanson. 2009. "Energy dissipation, flow resistance and gas-liquid interfacial area in skimming flows on moderate-slope stepped spillways." *Environ. Fluid Mech.* 9 (4): 427–441. <https://doi.org/10.1007/s10652-009-9130-y>.
- Felder, S., and H. Chanson. 2013. "Aeration, flow instabilities, and residual energy on pooled stepped spillways of embankment dams." *J. Irrig. Drain. Eng.* 139 (10): 880–887. [https://doi.org/10.1061/\(ASCE\)IR.1943-4774.0000627](https://doi.org/10.1061/(ASCE)IR.1943-4774.0000627).
- Felder, S., and H. Chanson. 2014. "Effects of step pool porosity upon flow aeration and energy dissipation on pooled stepped spillways." *J. Hydraul. Eng.* 140 (4): 04014002. [https://doi.org/10.1061/\(ASCE\)HY.1943-7900.0000858](https://doi.org/10.1061/(ASCE)HY.1943-7900.0000858).
- Frizell, K. W., F. M. Renna, and J. Matos. 2013. "Cavitation potential of flow on stepped spillways." *J. Hydraul. Eng.* 139 (6): 630–636. [https://doi.org/10.1061/\(ASCE\)HY.1943-7900.0000715](https://doi.org/10.1061/(ASCE)HY.1943-7900.0000715).
- Gonzalez, C. A. 2005. "An experimental study of free-surface aeration on embankment stepped chutes." Ph.D. thesis, Dept. of Civil Engineering.
- Gonzalez, C. A., and H. Chanson. 2004. "Interactions between cavity flow and main stream skimming flows: An experimental study." *Can. J. Civ. Eng.* 31 (1): 33–44. <https://doi.org/10.1139/03-066>.
- Gonzalez, C. A., and H. Chanson. 2006. "Flow characteristics of skimming flows in stepped channels. Discussion." *J. Hydraul. Eng.* 132 (4): 432–433. [https://doi.org/10.1061/\(ASCE\)0733-9429\(2006\)132:4\(432\)](https://doi.org/10.1061/(ASCE)0733-9429(2006)132:4(432)).
- Gonzalez, C. A., and H. Chanson. 2007. "Hydraulic design of stepped spillways and down-stream energy dissipators for embankment dams." *Dam Eng.* 17 (4): 1–18.
- Gonzalez, C. A., and H. Chanson. 2008. "Turbulence and cavity recirculation in air-water skimming flows on a stepped spillway." *J. Hydraul. Res.* 46 (1): 65–72. <https://doi.org/10.1080/00221686.2008.9521843>.
- Leonardi, S., P. Orlandi, and R. A. Antonia. 2007. "Properties of d- and k-type roughness in a turbulent channel flow." *Phys. Fluids* 19 (12): 125101. <https://doi.org/10.1063/1.2821908>.
- Matos, J. 1999. "Emulsão de ar e dissipação de energia do escoamento em descarregadores em degraus" [Air entrainment and energy dissipation in flow over stepped spillways]. [In Portuguese.] Ph.D. thesis, IST.
- Matos, J. 2000. "Hydraulic design of stepped spillways over RCC dams." In *Proc., Int. Workshop on Hydraulics of Stepped Spillways*, edited by H. E. Minor, and W. H. Hager, 187–194. Rotterdam, Netherlands: Balkema Publisher.
- Meireles, I. 2011. "Hydraulics of stepped chutes: Experimental-numerical-theoretical study." Ph.D. thesis, Departamento de Engenharia Civil, Universidade de Aveiro.
- Meireles, I., F. Renna, J. Matos, and F. A. Bombardelli. 2012. "Skimming, nonaerated flow on stepped spillways over roller compacted concrete dams." *J. Hydraul. Eng.* 138 (10): 870–877. [https://doi.org/10.1061/\(ASCE\)HY.1943-7900.0000591](https://doi.org/10.1061/(ASCE)HY.1943-7900.0000591).
- Ohtsu, I., Y. Yasuda, and M. Takahashi. 2004. "Flow characteristics of skimming flows in stepped channels." *J. Hydraul. Eng.* 130 (9): 860–869. [https://doi.org/10.1061/\(ASCE\)0733-9429\(2004\)130:9\(860\)](https://doi.org/10.1061/(ASCE)0733-9429(2004)130:9(860)).
- Perry, A. E., W. H. Schofield, and P. N. Joubert. 1969. "Rough wall turbulent boundary layers." *J. Fluid Mech.* 37 (2): 383–413. <https://doi.org/10.1017/S0022112069000619>.
- Rajaratnam, N. 1990. "Skimming flow in stepped spillways." *J. Hydraul. Eng.* 116 (4): 587–591. [https://doi.org/10.1061/\(asce\)0733-9429\(1990\)116:4\(587\)](https://doi.org/10.1061/(asce)0733-9429(1990)116:4(587)).
- Stephenson, D. 1988. "Stepped energy dissipators." In *Proc., Int. Symp. on Hydraulics for High Dams*. Beijing: IAHR.
- Takahashi, M., Y. Yasuda, and I. Ohtsu. 2008. "Flow patterns and energy dissipation over various stepped chutes. Discussion." *J. Irrig. Drain. Eng.* 134 (1): 114–116. [https://doi.org/10.1061/\(ASCE\)0733-9437\(2008\)134:1\(114\)](https://doi.org/10.1061/(ASCE)0733-9437(2008)134:1(114)).
- Toombes, L. 2002. "Experimental study of air-water flow properties on low-gradient stepped cascades." Ph.D. thesis, Dept. of Civil Engineering, Univ. of Queensland.
- Toombes, L., and H. Chanson. 2008. "Flow patterns in nappe flow regime down low gradient stepped chutes." *J. Hydraul. Res.* 46 (1): 4–14. <https://doi.org/10.1080/00221686.2008.9521838>.
- Wuthrich, D., and H. Chanson. 2014. "Hydraulics, air entrainment and energy dissipation on gabion stepped weir." *J. Hydraul. Eng.* 140 (9): 04014046. [https://doi.org/10.1061/\(ASCE\)HY.1943-7900.0000919](https://doi.org/10.1061/(ASCE)HY.1943-7900.0000919).
- Zhang, G., and H. Chanson. 2016a. "Gabion stepped spillway: Interactions between free-surface, cavity, and seepage flows." *J. Hydraul. Eng.* 142 (5): 06016002. [https://doi.org/10.1061/\(ASCE\)HY.1943-7900.0001120](https://doi.org/10.1061/(ASCE)HY.1943-7900.0001120).
- Zhang, G., and H. Chanson. 2016b. "Hydraulics of the developing flow region of stepped spillways. I: Physical modeling and boundary layer development." *J. Hydraul. Eng.* 142 (7): 8. [https://doi.org/10.1061/\(ASCE\)HY.1943-7900.0001138](https://doi.org/10.1061/(ASCE)HY.1943-7900.0001138).